Monitoring ecosystem restoration of multiple surface coal mine sites in China via Landsat images on Google Earth Engine

Huihui Wang [1], Miaomiao Xie [1, 2], Hanting Li [1], Qianqian Feng [1], Cui Zhang [1]

[1]School of Land Science and Technology, China University of Geosciences (Beijing), Beijing, China

[2]Key Laboratory of Land Consolidation, Ministry of Natural Resources of the PRC, Beijing, China

Correspondence

Miaomiao Xie, School of Land Science and Technology, China University of Geosciences (Beijing), Beijing100083, China

Key Laboratory of Land Consolidation, Ministry of Natural Resources of the PRC, Beijing100035, China

E-mail: xiemiaomiao@cugb.edu.cn

Funding resource

the National Key Research and Development Project of China, Grant/Award Number:2017YFC0504401.

Highlights

- Mine Landscape Restoration Index is proposed for monitoring mine site restoration,
- Restoration effects for 46 surface coal mine sites in the northwestern ecologically fragile region of China were detected.
- MLRI time series can be used to describe the spatial distribution and trend projection of mine site restoration.
- Google Earth Engine platform and Landsat images help in large-scale multiple mine restoration monitoring.

Running title

Monitoring ecosystem restoration of multiple surface coal mine sites based on Google Earth Engine

Acknowledgments

This study was financially supported by the National Key Research and Development Project of China (2017YFC0504401).

Abstract

The restoration of surface mining is a key to meet the global ecosystem restoration target. With increased data accessibility and computing tool capabilities, it becomes possible to expand mine restoration monitoring from single mine sites to multiple mine sites on a large scale. This study constructed a new index, Mine Landscape Restoration Index (MLRI), by coupling Land Surface Temperature (LST) and Enhanced Vegetation Index (EVI) to simultaneously monitor the restoration of regional multiple mine sites. We analyze historical and future trends of restoration using Mann-Kendall test, Sen' slope, and Hurst exponent for MLRI time series. The restoration effects of 46 surface coal mine sites located in the northwestern ecologically fragile region of China from 2000 to 2019 were assessed, based on 3675 Landsat images on Google Earth Engine. The results showed that MLRI was effective in identifying restoration areas and processes in surface mine sites, which was validated by high-resolution images and field investigation of mine samples. The restoration area overall percentage was significantly higher in mines started mining before 2000 than after 2000. According to the restoration effects, we clustered the 46 sites into high, medium, and low restoration area percentage clusters with 13, 11, and 22 mine sites, respectively. Individual clusters have aggregation characteristics within each mine region, but are distributed irregularly across the different six mine regions. This study provides a new approach to monitoring the restoration of surface coal mine sites and inform government managers in developing mine restoration programs and sustainable mining development plans.

Keywords

Surface coal mining

Restoration Monitoring

Mine Landscape Restoration Index

Time series

Restoration effect

Google Earth Engine

1.Introduction

In comparison to any comparable period in human history, humans have changed the Earth's ecosystems more rapidly and extensively since the 1950s (Millennium Ecosystem Assessment, 2005). The diversification and intensification of land use and technological advances have led to rapid changes in hydrological processes, biogeochemical cycles, and landscape dynamics (International Geosphere-Biosphere Programme, 2005). Among these changes, land degradation, destruction of vegetation and loss of biodiversity caused by the mining industry affect the provision of ecosystem services, thus affecting human well-being and sustainable development (Bian & Lu, 2012; Feng, Wang, Bai, & Reading, 2019; Wu, Lv, Zhao, Sun, & Li, 2020). In the 21st century, people are beginning to focus on sustainable mining (Moomen, Bertolotto, Lacroix, & Jensen, 2019). Ecological restoration is seen as one of the main strategies that the global community must pursue in this century, and mine site restoration is an important part of it (Hobbs & Harris, 2001; Intergovernmental Science-Policy Platform on Biodiversity and Ecosystem Services, 2018). In order to enhance the United Nations Sustainable Development Goals and sustainable mining plans of countries, it is essential to establish restoration effects monitoring datasets for mine sites in large geographic areas (Moomen et al., 2019; United Nations, 2015). Simultaneous restoration monitoring of the region's mine sites will provide a clear picture of the overall state of restoration in the policy context, which will contribute to the sustainable development of the region and even the country, and thus meet the sustainable development requirements of human society.

Simultaneous monitoring of large-scale multiple mine sites restoration is challenged by efficiency, feasibility, and reliability. In traditional monitoring of surface coal mine sites, researchers have collected soil and observe plant and biodiversity in the field (Freitas et al., 2019; Huang, Zhang, Hu, & Zhao, 2016). The datasets resulting from these efforts provide a

reliable tool for examining and verifying the occurrence and effects of ecological restoration at a mine site. However, it is not efficient and feasible on a large scale because of budgetary and personnel limitations (Zhou, Okin, & Zhang, 2020). With the advancement of satellite earth observation technology, remote sensing has become an effective monitoring tool (Song, Song, Gu, & Li, 2020). Fast and efficient remote sensing technology and high-resolution remote sensing data can provide timely, objective, and high-precision data support for mine site restoration monitoring (Karan, Samadder, & Maiti, 2016).

In surface mine sites, mining activities and ecological restoration directly impact on land use and vegetation cover (Sen, Zipper, Wynne, & Donovan, 2012). Currently, mine restoration monitoring mainly uses high-resolution images to find out the image characteristics, distribution, and change rules of the restored vegetation in mine sites and establish decipherment signs for decipherment. Such interpretive mapping has advantages in reliably and efficiently identifying mine site restoration. But limitations on the tracking of restoration processes may constrain its utility in assessing long-term environmental impacts and sustainability (Yang et al., 2018). Recent researches have adopted time-series analysis to monitor mine site restoration processes (Xiaoyang Liu, Zhou, & Bai, 2016; Song et al., 2020). Yang et al. (2018) mapped vegetation disturbance and restoration at the Curragh coal mine site in Australia over a long term using the LandTrendr algorithm and Landsat images. Vidal-Macua, Nicolau, Vicente, and Moreno-de Las Heras (2020) tried to assess restoration in surface coalfield by machine learning method. These researches combined reliability and efficiency in monitoring restoration process within a single mine site and depicted extensive details of the restoration process. However, due to the parameters set at specific mine sites, it remains a challenge in feasibility to expand these methods to for monitoring restoration in multiple mine sites on a large scale. Hence, it is necessary to explore new restoration monitoring methods suitable for multiple mine sites on a large scale.

The MODIS Global Disturbance Index (MGDI) can effectively monitor ecosystem dynamics by combining MODIS Land Surface Temperature (LST) and Enhanced Vegetation Index (EVI) data and provides a feasible idea for large-scale monitoring (Mildrexler, Zhao, & Running, 2009). It was established based on the coupling of LST and Vegetation Index (VI), which has more biophysical and processes properties than VI for a more complete characterization of the land cover (Mildrexler, Zhao, Heinsch, & Running, 2007; Mildrexler et al., 2009). The basic principle behind this technique is that as the density of vegetation increases, the surface temperature decreases through latent heat conduction. However, the 1km resolution of MGDI is unsuitable to apply to monitor with a mine site. In our previous research, we have constructed a Dump Reclamation Disturbance Index (DRDI) in combination with Landsat LST and Landsat EVI based on MGDI (Xie et al., 2019). The DRDI can effectively identifies the disturbance of reclamation dump by amplifying the disturbance signal. In this study, we construct a Mine Landscape Restoration Index (MLRI) based on MGDI and DRDI to identify ecological restoration in the complex environment of the mine site. Google Earth Engine (GEE) platform has a wide range of applications in both environmental and social remote sensing, and researchers have shared many mature algorithms (Wang et al., 2020). Therefore, we calculated the LST and EVI data for MLRI construction on GEE platform.

As the world's largest producer and consumer of coal, most of China's fourteen large coal bases locate in the northwestern China, which is an fragile region (International Energy Agency, 2020; Zhang, Wang, Bai, & Lv, 2015). There are many expanding surface coal mines in the region, making the conflict between coal development and the surrounding environment/ecosystem services function increasingly evident (Yu et al., 2018). There is an urgent need to monitor the restoration of multiple mines in the region to support the sustainable development of the region and the country. Thus, the main objectives of our study

are following: (1) to propose an index which is sensitive to the incremental process of restorative changes based on the GEE platform; (2) to analyze the restoration effects of 46 large surface coal mine sites which are in the northwestern ecologically fragile region of China from 2000-2019.

2. Study areas and methods

2.1. Study area

Coal resources are an important material basis for economic and social development. However, mining activities are one of the most serious human activities affecting the economy and the environment, and in particular, surface coal mining causes great pressure on the ecological environment (Hilson, 2002; Yu et al., 2018). According to “the Thirteenth Five-Year Plan for the Development of the Coal Industry” published by the National Energy Administration (NEA) of China, the general layout of China's coal development is to compress production in the east, limit production in the mid and north-east, and optimize the west (National Energy Administration, 2016). In the northwest ecologically fragile region of China, where coal resources are abundant and mining conditions are good, but the ecological environment is fragile, the surface coal mine sites restoration deserves attention.

2.1.1 Selection of mine sites

In this study, the national mine dataset on the Resource and Environment Science and Data Center (RESDC) was used to acquire mine names, coordinates, mining methods, and mine species. The "National Coal Mine Production Capacity Report" of the NEA, publicly available company information, and relevant literature were used to assist in verifying the accuracy of the mine information (H. Li, She, Zhou, & Huang, 2019; National Energy

Administration, 2019). Finally, a total of 46 surface coal mine sites located in the northwestern ecologically fragile region of China were selected for study. These mine sites are in Inner Mongolia, Xinjiang, Shanxi, Shaanxi, Ningxia, Xinjiang provinces (Fig. 1). At the end of 2018, the 46 surface coal mine sites have a production capacity of about 450 million t/a, accounting for about 70% of all producing surface coal mines in China.

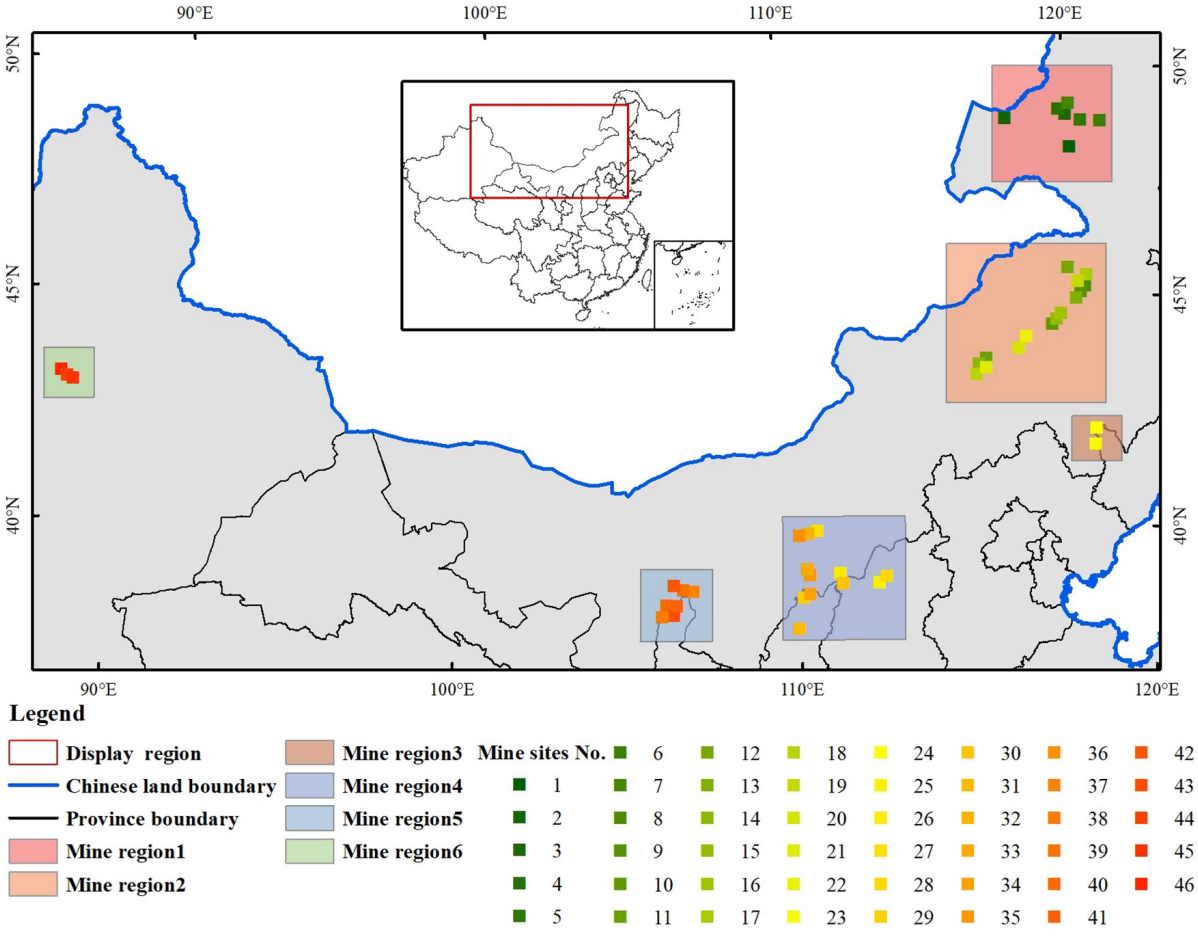

FIGURE 1 Mines mapped and analyzed in this study. The names of the six mine regions are: mine region1 = Hailar region, mine region 2 = Shengli&Huolinhe region, mine region3 = Yuanbaoshan region, mine region4 = Shanbeimengnan region, mine region5 = Zhuozishan&Luotuoshan region, mine region6 = Zhunnan region.

2.1.2 Mine site mapping

Since the geographic location of a mine is stored as a central coordinate point in the

national mine dataset, we used Google Earth's high-resolution imagery and built-in mapping tools to map the extents (Werner et al., 2020). As the central area of the mine site is the focus and challenge of restoration, only open pits, dumps, and structures that are immediately adjacent to and significantly associated with the mining activity would be considered to within the mine extent (Werner et al., 2020). To ensure that the extent of mine sites that have undergone ecological restoration is accurately identified, we have retraced sufficient historical images in the mapping process. When the extent of adjoining mines could not be distinguished (using common dumps), they were mapped as one mine area. Besides, in order to compare the restoration effects of mine sites with different mine durations, the time of mining start was counted, which can be easily obtained from the company's public information on the website. To facilitate data processing and based on the distribution of mines, the 46 mines have been divided into 6 mine regions (Table 1).

TABLE 1 Mine sites information of this study.

Mine regions	No.	Mine Site name	Area/hm^2	Mining start time
Hailar region	1	Yimin	2887.64	Before 2000
(Mine region1,7 mine sites)	2	Lingquan	2876.34	Before 2000
	3	BaorixileI	2297.88	Before 2000
	4	BaorixileII	733.99	2004
	5	Zhanihe	702.63	2010
	6	Mianduhexi	409.29	Before 2000
	7	Xieertala&Shunxing	299.95	Before 2000
Shengli&Huolinhe region	8	Huolinhenan	5053.58	Before 2000
(Mine region2,15 mine sites)	9	Zhahanaoer	4116.16	Before 2000
	10	BaiyinhuaI&II	3654.87	2008
	11	ShenglidongII	3549.61	2008
	12	Hesigelawu	3104.06	2008
	13	Baorihushuo	2368.73	2006
	14	ShenglixiI	2183.69	Before 2000
	15	BaiyinhuaIII	1928.56	2009

	16	BaiyinhuaIV	1585.40	2009
	17	Fengyang	1550.27	Before 2000
	18	Shenglixier	1452.53	2007
	19	Huolinhebei	1121.31	Before 2000
	20	JilinguoleII	802.80	2011
	21	ShenglixiIII	533.96	2008
	22	Hadatu	311.84	Before 2000
Yuanbaoshan region	23	Pingzhuangxi	1758.22	Before 2000
(Mine region3, 2mine sites)	24	Yuanbaoshan	1613.96	Before 2000
Shanbeimengnan region	25	Anjialing&Antaibao	8268.35	Before 2000
(Mine region4, 12 mine sites)	26	Heidaigou&Haerwusu	5729.04	Before 2000
	27	Daqingshan	4481.39	2010
	28	Pingshuodong	2044.90	2008
	29	Wujiata	1822.38	Before 2000
	30	Weijiamao	992.34	2012
	31	Xiwan	925.06	2016
	32	Dongshanwan	491.39	2010
	33	Datangbaoli	355.15	2007
	34	Majiata	265.42	Before 2000
	35	Bijian	228.12	2010
	36	Shuiquan	201.63	2008
Zhuozishan&Luotuoshan region	37	Luotuoshan	25941.68	Before 2000
(Mine region5, 7 mine sites)	38	Dafeng	10305.08	Before 2000
	39	Haibowan	5569.27	Before 2000
	40	Maliantan	3111.36	Before 2000
	41	Caiyuangou	1074.46	Before 2000
	42	HaibowanII	420.82	2007
	43	Qingshuigou	263.99	Before 2000
Zhunnan region	44	Heishan	1144.35	Before 2000
(Mine region6, 3 mine sites)	45	Heishanxiao	913.99	2009
	46	Tuokexun	371.85	2009

Fig. 2 shows two example extents of the Antaibao&Anjialing (Image date June 11, 2019) and ShenglixiIII (Image date June 11, 2019) mapped on Google Earth platform. The left figure shows Antaibao&Anjialing mine site, with mine central coordinate point of 39°30′N，112°22′E and a mine area of 8268.35hm^2, which was put into operation in 1987 and the abandoned dumps had been undergoing restoration since 1994. The right figure shows

ShenglixiIII, with mine central coordinate point of 43°58′N ， 115°60′E and a mine area of 533.96hm^2, which was put into operation in 2008.

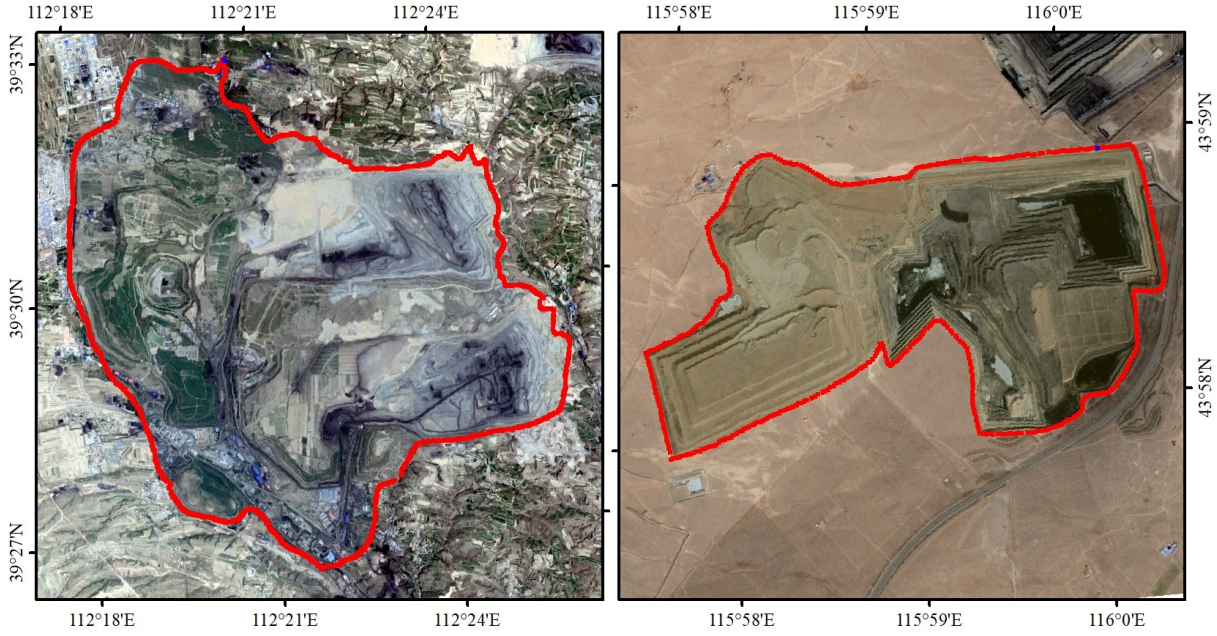

FIGURE 2 Surface mine site extents of Antaibao&Anjialing (left) and ShenglixiIII (right).

2.2. Data resources

In this study, besides the national mine datasets and Google Earth images, a total of 3675 images were used from June to September each year from 2000 to 2019 on GEE platform (https://earthengine.google.org/). Landsat 5 Surface Reflectance (SR) images were used from 2000 to 2011 and Landsat 8 SR images from 2013 to 2019. Landsat7 images from 2012 were not used because of gaps in the images. These images have been pre-processed for atmospheric correction, radiometric calibration, and the FMask algorithm was used to mask of clouds, cloud shadows, ice, and snow.

2.3. Construction of the Mine Landscape Restoration Index

2.3.1 The meaning of mine landscape restoration

Landscape Restoration means the consequence of restoring degraded ecosystems, which is

used to monitor the trajectory of the ecosystem. The term "restoration" as used in this study is like the terms: "rehabilitation", "reclamation", "revegetation", and "revitalization", which appearing in other studies (Cross et al., 2018; Hu, 2019). We did not distinguish the method of restoration but focus on the consequence of restoration in different periods, which is the timely restoration of degraded ecosystems disturbed by mining activities and mitigating the conflict between the extraction of mineral resources and the surrounding environment/ecosystem. Ecological restoration of mine sites requires multiple levels, such as land levelling, improvement of soil physical and chemical properties, and revegetation. However, both land levelling and soil improvement measures are aimed at providing a better environment for vegetation to grow, thus increasing the resilience of the ecosystem, and ultimately achieving the goal of positive ecosystem succession (Bruno Rocha Martins et al., 2020; Macdonald et al., 2015).

2.3.2 Mine Landscape Restoration Index

Mildrexler et al. (2009) discussed the potential of using the LST/EVI ratio not only to identify wildfire disturbance, but also in more moderate vegetation changes such as deforestation and insect invasions. In one mine site, when the ecosystem was disturbed, the degradation of surface vegetation led to severe disruption of the vegetation structure and a decrease in EVI values. The reduction in surface vegetation leads to a corresponding reduction in evapotranspiration, resulting in an increase in LST (Nemani & Running, 1997; Xie et al., 2019). Conversely, when mine restoration takes place, the improved condition of surface vegetation leads to an increase in EVI values and a decrease in LST values. The better the restoration effect in a mine site, the more significant the cooling effect of the vegetation. The LST, which indicates vegetation function, and the EVI, which indicates vegetation structure, were coupled to construct a landscape restoration index for the mine site to reflect

restoration effects. EVI was chosen to avoid saturation of NDVI in areas of high biomass restoration areas, which is important for monitoring change trends (Mildrexler et al., 2009). The 46 mines in this study are all located in the arid and semi-arid region of northwest China and have similar climatic conditions.

$$MLRI_{ij} = \frac{LST_{j\max} / EVI_{j\min}}{LST_{ij} / EVI_{ij}} \quad (1)$$

Where $MLRI_{ij}$ is the MLRI value of pixel j in the year i; LST_{ij} and EVI_{ij} are the maximum June to September composite LST and EVI values of pixel j in the year i, respectively; LST_{jmax} and EVI_{jmin} are maximum value of LST and minimum value of EVI of annul maximum June to September composite of pixel j from 2000 to the year i, respectively. The ratio of LST_{jmax} to EVI_{jmin} represents the worst growth condition of the vegetation in the time series, and the ratio of LST_{ij} and EVI_{ij} represent vegetation growth condition of the year i. The ratio of the worst condition to condition in year the i is used to characterizing the degree of restoration of pixel j in year i. For example, to calculate the 2010 MLRI value of the j pixel, use the LST_{jmax}/EVI_{jmin} from 2000 to 2010 divided by the 2010 LST_j/EVI_j. The minimum value of MLRI is 1, and a higher value indicates a better degree of restoration.

LST and EVI are calculated using Landsat 5/8 SR images on the GEE platform. Annual LST and EVI are the maximum composite values for all images from June to September each year. Radiative transfer equation was used to calculate LST (Sobrino, Jiménez-Muñoz, & Paolini, 2004; United States Geological Survey, 2016). To improve the quality of data, the annual EVI and LST values are EVI and LST maximum composites for all images from June to September of each year. The construction of MLRI is implemented on the local computer's ArcGIS10.2 platform.

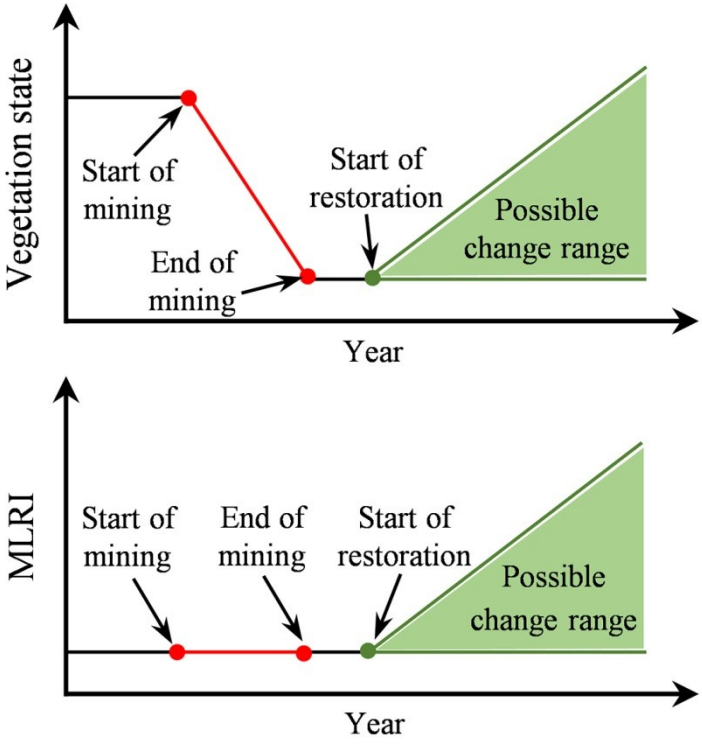

FIGURE 3 A conceptual model for the trajectory of vegetation state and MLRI for a pixel.

In a pixel range, vegetation state declines rapidly when it is disturbed by mining and slowly recovers after restoration begins. The rate and quality of recovery are determined by the degree of disturbance, the resilience of the native ecosystem and the effectiveness of the restoration project. The interval between disturbance and recovery is shortened with the implementation of the Concurrent Mining and Reclamation technology. Such change is often difficult to monitor with common vegetation indices. MLRI based on MGDI and DRDI constructed for mine sites narrow the sensitivity to disturbance and increase the sensitivity to restoration occurrence. At the same time, MLRI uses the current state of the pixel itself to compare with the historical state, which helps to avoid differences due to background conditions. Thus, MLRI contributes to identify non-simultaneous restoration and restoration processes easily and sensitively of multiple surface coal mine sites on a large scale.

2.4 Restoration identification and classification

The changes in MLRI values from 2000 to 2019 for the 46 mine sites were analyzed by

Mann-Kendall test and Sen's slope trend to indicate the restoration process and identify restoration areas. The Hurst exponent was further analyzed the long-term temporal dependence of the MLRI time series. Based on the results of Mann-Kendall test, Sen's slope, and Hurst exponent, 46 mine sites' restoration areas were identified and restoration types were classified.

Parametric and non-parametric methods are the main tests used to detect important trends in time series. The data need to be independent and normally distributed in parametric trend tests, whereas in non-parametric trend tests, only the data need to be independent. In this study, we used two non-parametric tests, Mann-Kendall test, and Sen's slope, to detect change trends of MLRIs (S. Liu et al., 2019). The Mann-Kendall test can effectively distinguish whether a process is undergoing natural fluctuations or a definite trend of change (Z. Zhou et al., 2020). We used the Mann-Kendall test to eliminate noise from climate change with a natural state. The test statistic Z of the Mann-Kendall test was adopted to test the significance of the MLRI trend. The confidence level α was set as 0.05, $|Z|>1.96$ indicates that there is a significant change in the MLRI time series (Kendall, 1970; Mann, 1945). For non-significant changes, some of the trends nearly exhibited no change. A positive Sen' slope value indicates that the changing trend of MLRI in a pixel is beneficial and that the mine ecosystem gradually becomes recovered; by contrast, a negative value indicates that the changing trend is decreasing, i.e. the landscape condition gradually deteriorates. Accordingly, four kinds of classification results were obtained through trend analyses: (1) $|Z|>1.96$ and $Slope>0$ indicates a Significant Increase (SI) trend; (2) $|Z|\leq1.96$ and $Slope>0$ indicates an Non-significant Increase (NI) trend; (3) $|Z|\leq1.96$ and $Slope\leq0$ indicates a Non-significant Decrease (ND) trend; (4) $|Z|>1.96$ and $Slope\leq0$ indicates a Significant Decrease (SD) trend. In this study, the SI trend of MLRIs indicates the presence of a restoration process in an area, and areas with NI and ND trends not experiencing significant restoration and disturbance, whereas the SD

indicates that the area is experiencing ongoing disturbance, resulting in a continued decline in vegetation state.

R/S analysis was proposed by Hurst in the study of hydrological observations as a fractal theory for quantitatively describing the dependence of time series, and is widely used in economics, hydrology, geology, and climatology (Peng, Liu, Liu, Wu, & Han, 2012; Z. Zhou et al., 2020). And H-value is the result of Hurst exponent analyses, which ranged from 0 to 1. If the value is smaller than 0.5, the future trend of time serious is opposite to the past. The smaller the H-value, the stronger the anti-consistency. The value equals 0.5 means that the time series is a random independent sequence. If the value is greater than 0.5, the time series shows consistency, and the future trend of time series is the same as the past. The greater the H-value, the stronger the consistency. In this study, H-value > 0.5 was used to characterize the consistency of landscape restoration trends, with H-value≤0.5 indicating anti-consistency.

Areas with MLRI SI trends are classified into two restoration types, SCI, and SAI, based on their H-values (Table 2). The SCI area represents the consistency of future trends in the restored area. And the SAI area signals the anti-consistency of future trends in the restored area, requiring improved restoration or more ecological stewardship.

TABLE 2 Principles of Restoration types classification.

Restoration types	Mann-Kendall test	Slope	H-value
Significant Consistent Increase (SCI)	>|1.96|	>0	>0.5
Significant Anti-consistent Increase (SAI)			≤0.5

2.5 Accuracy assessment and validation

In order to verify the accuracy of the MLRI time series in identifying the mine restoration area, we chose two sample mine sites for accuracy assessment and validation because it was difficult to find suitable high-resolution images of all mine sites. This study uses Google Earth's high-resolution images to verify the accuracy of the restoration identified of

Antaibao&Anjialing mine site, which started mining before 2000, and ShenglixiIII mine site, which started mining after 2000. The accuracy was analyzed using a confusion matrix to calculate producer accuracy, user accuracy, overall accuracy, and Kappa coefficients. Furthermore, we field-validated the identified restoration areas of Antaibao&Anjialing, with detailed data in the supporting material.

Among the 600 random points (pixels) in the Antaibao&Anjialing, 377 of the 383 points restored that were actually present were identified, while 189 of the 217 points that were not restored were identified. Among the 100 random points (pixels) in the ShenglixiIII , 13 of the 15 points restored that were actually present were identified, while 82 of the 85 points that were not restored were identified. The accuracy of the confusion matrix calculations for restoration identification is shown in table 3. The overall classification accuracy of the Antaibao&Anjialing is 0.94, with a Kappa coefficient of 0.88; the overall identification accuracy of the ShenglixiIII is 0.95, with a Kappa coefficient of 0.81 (Table 3). Both mines had only a few of false restoration identification points.

TABLE 3 The accuracy of the detected restoration

Mine site	Significant increase		Other trends		Overall accuracy	Kappa coefficient
	Producer's accuracy	User's accuracy	Producer's accuracy	User's accuracy		
Antaibao&Anjialing	0.98	0.93	0.87	0.97	0.94	0.88
ShenglixiIII	0.81	0.86	0.98	0.96	0.95	0.81

2.6 Other analysis methods

The Kruskal-Wallis (K-W) test is a non-parametric test that was adopted to resolve whether there was a significant difference between in the area percentage of restoration types between mine sites. This study uses Spearman's correlation analysis to explore whether there is a relationship between the ecological restoration status of mine sites and the duration of

mining. Mining duration was calculated by using 2019 minus the mining start year. Area percentages of restoration types were clustered using K-means clustering algorithm to analyze their characteristics.

3.Results

The MLRIs of all the 46 mine sites were calculated and mapped for each year from 2000 to 2019, and the areas of restoration were identified and classified into different restoration types.

3.1 Restoration effects for 46 mining sites

3.1.1 Restoration effects

The proportion of restoration area indicated the restoration status from a holistic perspective. For the 24 mines that began mining before 2000, 55.01% of the restoration area was identified (Fig. 4). 28.47% of the restoration area remained stable during the restoration process (SCI), while 26.54% of the restoration area was expected to be at risk of degradation (SAI). For the 22 mines that started mining after 2000, 36.68% of the area restored, 20.26% remained stable (SCI), and 16.42% were predicted to be at risk of degradation (SAI). Moreover, the average area percentages of SCI, SAI and SI for mines mined before and after 2000 passed the Kruskal-Wallis test ($P<0.01$), i.e., the percentage of restoration area was significantly higher in mines that started mining before 2000 than after 2000.

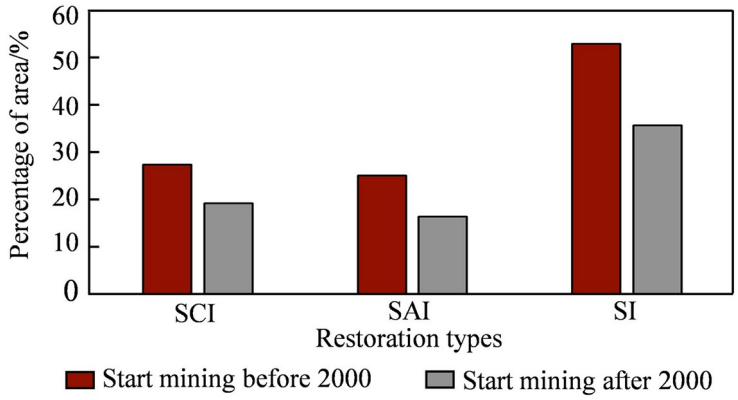

FIGURE 4 Area percentage of restoration types area different start mining time

3.1.2 Relationship between restoration effects and mining duration

The Spearman correlation coefficient indicated that there is a positive correlation between mine restoration effect and mining duration. Mining duration is calculated using the year 2019 minus the year mining beginning. For example, the mining duration is 11 years for mines that started in 2008 and 20 years for mines that started before 2000. The results showed that the Spearman correlation coefficients of SI, SCI, and SAI with mining duration were 0.309, 0.326, and 0.352 ($P<0.05$) for the 46 mines, respectively.

3.1.3 Clustering of restoration effects

According to the percentages of SCI and SAI area, the 46 mines were clustered into three clusters, with 13, 11, and 22 mine sites in Cluster 1, Cluster 2, and Cluster 3, respectively (Fig. 5). Individual clusters have some aggregation characteristics within each mine region, but are distributed irregularly across the different six mine regions. Three clusters passed the Kruskal-Wallis test ($p<0.01$), i.e., the three types differed significantly. Cluster 1 has the high restoration percentage, and the percentage of SCI area was greater than the percentage of SAI area. Cluster 2 had a medium restoration percentage, with a smaller percentage of SCI area than SAI. Moreover, cluster 3 had the low restoration percentage, with a similar proportion of SCI area as SAI.

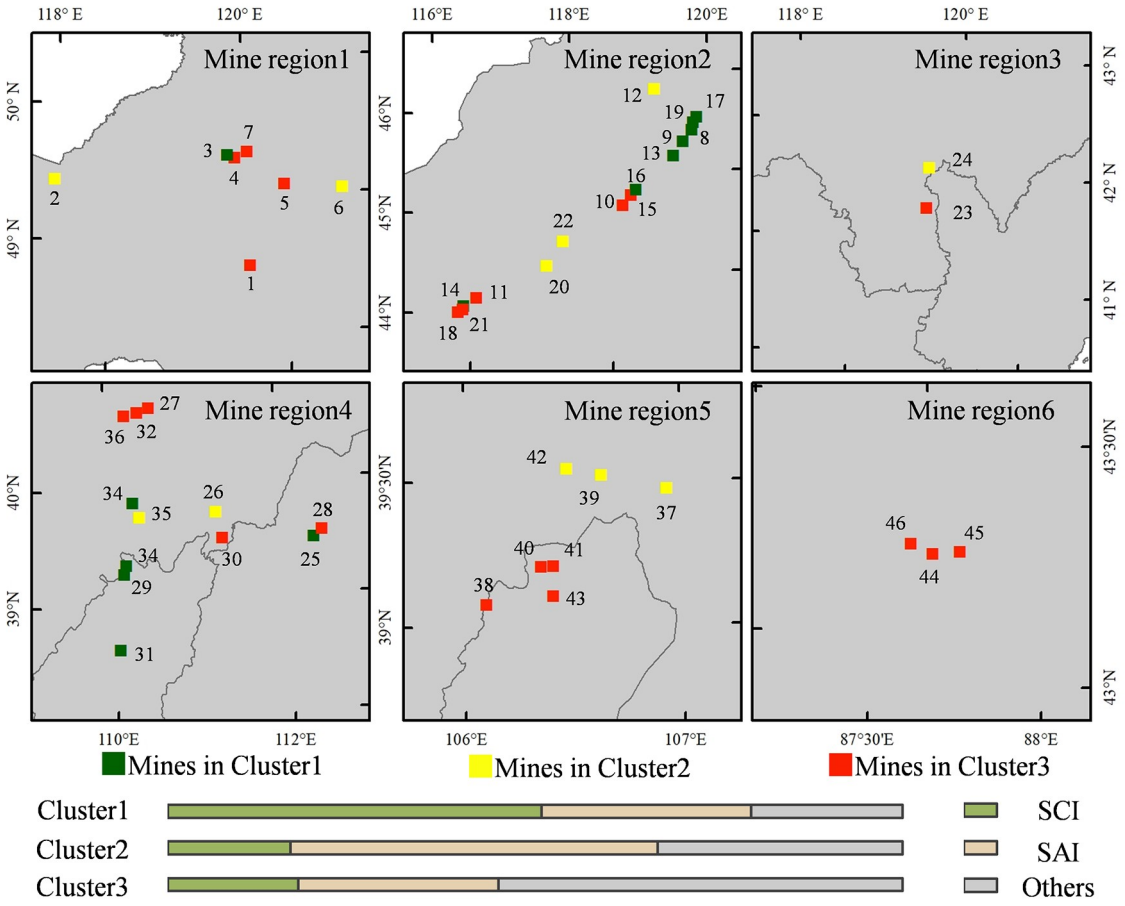

FIGURE 5 The distribution of mines in three clusters.

The mine sites with the highest restoration percentage are located mainly in mine region2 (Hailar) and mine region4 (Shanbeimengnan), which belong to cluster1 (Fig. 5). The mine sites in clusters 2 and 3 can be found in mine region1 to 5 (Hailar, Shengli&Huolinhe, Yuanbaoshan, Shanbeimengnan, and Zhuozishan&Luotuoshan), and all three mines in mine region6 (Zhunnan) are in Cluster 3. Although the mines in cluster 2 have a higher percentage of restoration, the percentage of SAI is higher than SCI, so enhanced stewardship of restored areas or improved restoration methods are needed. The percentage of restoration in Cluster 3 is low and effective mine site restoration needs to be enhanced in the future.

3.2 Mine restoration monitoring use MLRI in example

In addition to assessing the overall restoration effects in the previous section, the time

series analysis of the MLRI index can be used to express the spatial distribution of restoration types and locate the restoration status of different areas. Antaibao&Anjialing and ShenglixiIII were used as case studies to demonstrate the spatial distribution of restoration types.

3.2.1 Changes in MLRI of surface mine sites

The changes in the average MLRI values for the four areas with SI, NI, ND, and SD trends in the Antaibao&Anjialing and ShenglixiIII mine sites indicates that the restoration process has periods (Fig. 6). For those mine sites that began mining earlier than 2000, there are two periods, unobvious and obvious restoration periods. In the case of the Antaibao&Anjialing mine site, for example, the first period was from 2000 to 2009, with similar MLRI values in different areas, and the second period was after 2009, with significantly higher MLRI values in the restoration area. For mine sites which were developed later than 2000, there is also an additional period of natural state change, in which the MLRI values fluctuate similarly at the mine sites. For example, at ShenglixiIII, the period from 2000 to 2008 was a natural state fluctuation, while the period from the start of mining in 2008 to 2011 was a period of insignificant restoration, and after 2011 it was an obvious restoration period, where the MLRI value of the restoration area increased significantly. For both types of mine sites thatrera began mining earlier and later than 2000 , MLRI values in the SI areas were trending upwards and the identification of restoration processes was effectively identified. The NI and ND areas had small changes in MLRI values, i.e. were not effectively restored from mining activities. In the SD areas, which were continuously disturbed by mining, the MLRI values approached 1. Since the MLRI index is constructed to sensitively identify the restoration process, the two non-significant and significant decrease trends have a limitation in identifying disturbing situations.

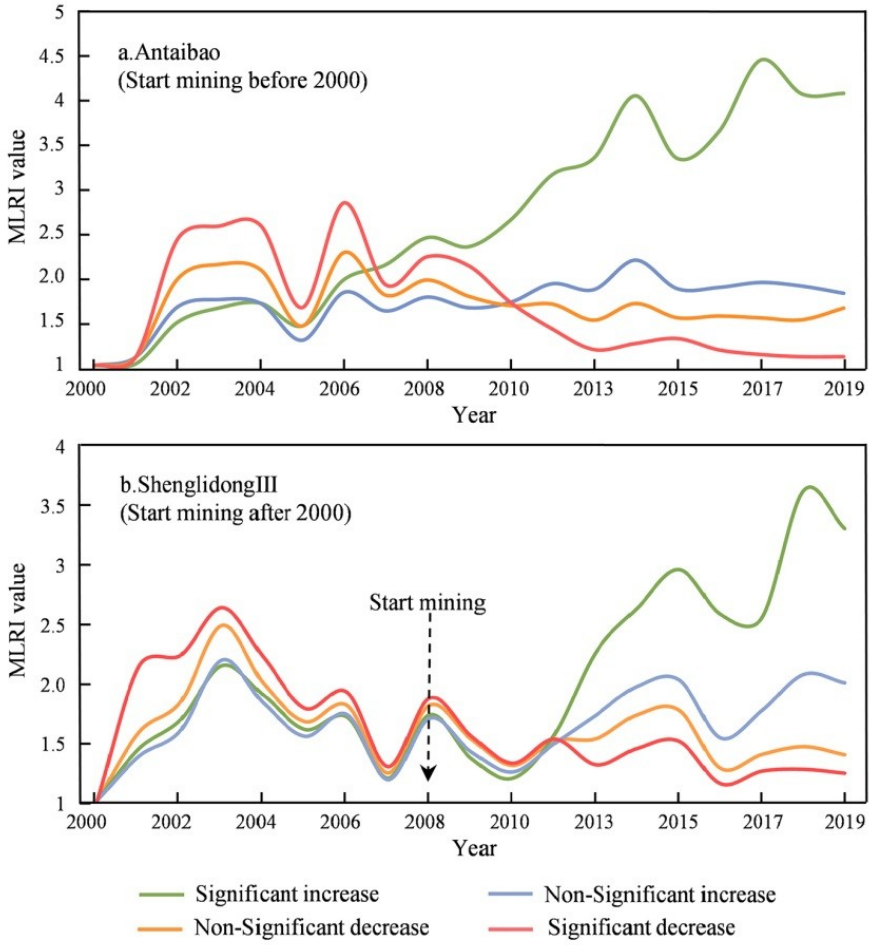

FIGURE 6 MLRI changes of Antaibao&Anjialing and ShenglixiIII.

3.2.2 Restoration types classification

Areas with the four MLRI trends exhibit apparent aggregation in their spatial distribution (Fig. 7a and Fig. 7b). In the Antaibao&Anjialing, areas of SI in MLRI values are mainly located in the western part of the site, where the abandoned dumps have been restored. The areas of NI, ND and SD in MLRI values are mainly located in the eastern, where is experiencing frequent mining activities (Fig. 7a). The areas of significant restoration in MLRI values at the ShenglixiIII are mainly in the western and southern abaundoned dumps. The areas of NI, ND and SD of MLRI values are mainly located in mining area and new dump (Fig. 7b).

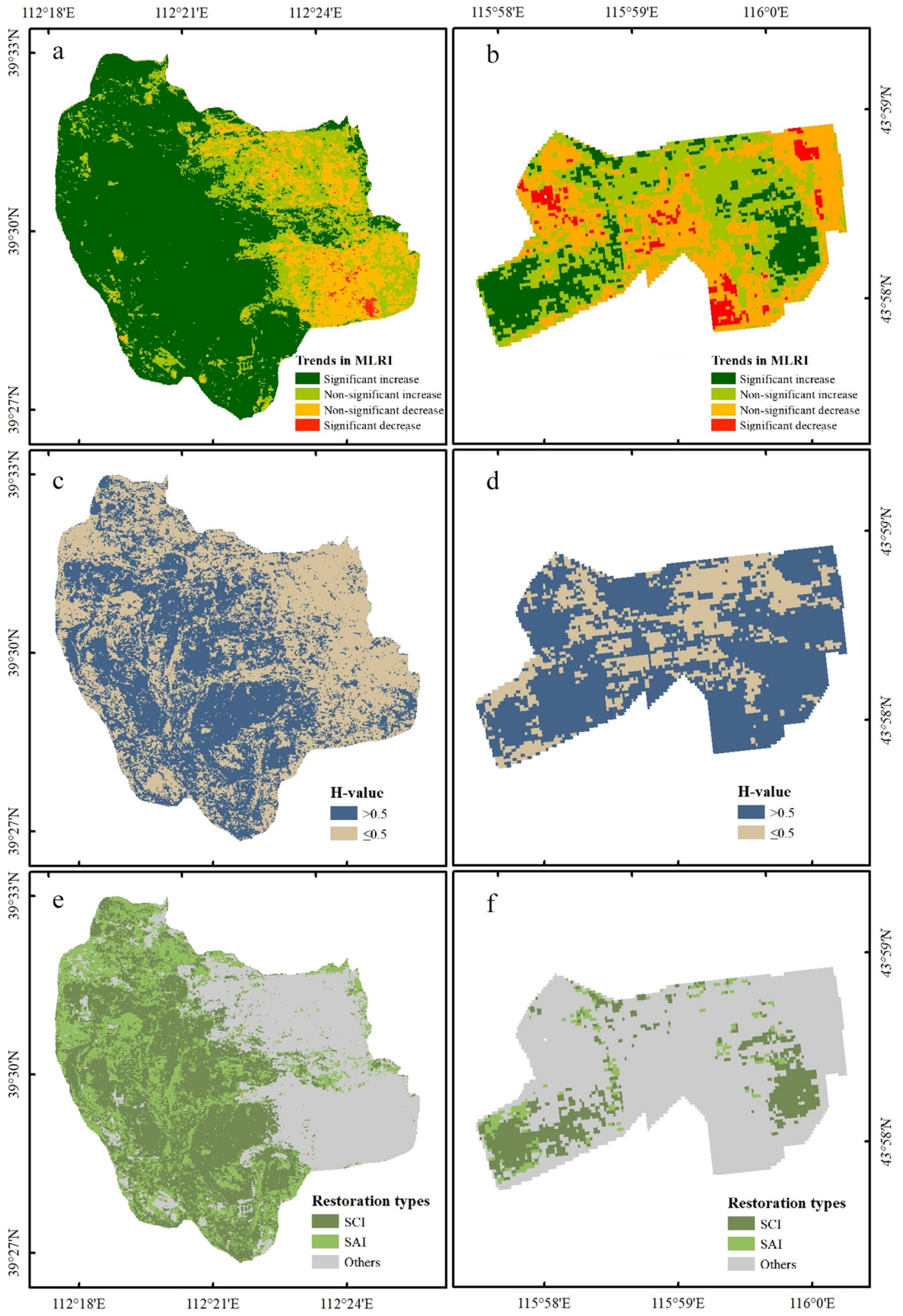

FIGURE 7 Details of the spatial distribution of restoration types of Antaibao&Anjialing (left) and

ShenglixiIII (right) from 2000 to 2019.

The Hurst exponent calculations for Antaibao&Anjialing and ShenglixiIII are shown in Fig. 7c and Fig. 7d. An H-value greater than 0.5 indicates a future trend consistent with history, while a value less than 0.5 indicates a future trend inconsistent with history. 53.76% of the area in the Antaibao&Anjialing mine site has an H-value greater than 0.5 and 46.24% has an H-value less than or equal to 0.5. In ShenglixiIII, 68.79% of the area has a Hurst exponent value greater than 0.5 and 32.21% has an H-value less than or equal to 0.5. The two areas with different H-values have distinct aggregation characteristics, with areas of Hurst Index values greater than 0.5 being mainly restored abandoned dumps, while areas of Hurst Index values less than or equal to 0.5 are main areas of frequent mining activity.

Areas with SI trend of MLRIs were identified as restoration areas and classified into two types according to Hurst index values: SCI and SAI. The area of SI, SCI, and SAI at Antaibao&Anjialing and ShenglixiIII as a percentage of the mine site area is shown in the table 4. The mining at Antaibao&Anjialing began earlier, so the restoration of the abandoned site began earlier. The area of SI at Antaibao&Anjialing is 64.25% of the entire mine area. Among which, SCI and SAI area accounted for 42.68% and 21.47% of the mine site area, respectively. The area of SI at the ShenglixiIII is 19.33%. Among which, SCI and SAI accounted for 14.94% and 4.39% of the mine site area, respectively.

TABLE 4 Percentages of the area of restoration types at Antaibao&Anjialing and ShenglixiIII mine sites

Restoration types	Antaibao&Anjialing	ShenglixiIII
	Percentage of area/%	Percentage of area/%
Significant consistent increase (SCI)	42.68	14.94
Significant anti-consistent increase (SAI)	21.47	4.39
Significant increase (SI)	64.25	19.33

4. Discussion

4.1 Reliability of surface coal mine sites restoration monitoring using Landsat data and MLRI

This study indicates the feasibility and reliability of using Landsat data to construct the MLRI for monitoring the restoration of surface coal mine sites in the northwestern ecologically fragile region of China from 2000 to 2019. The GEE platform was used for basic data processing as thousands of images in total need to be processed in mines located in different regions. The regional and global datasets of mine sites that have been developed from existing studies focus on the composition and expansion of mine sites (Werner et al., 2020; Yu et al., 2018). Currently, many studies have achieved monitoring of mine recovery processes, but they are mostly based on individual mine sites (J. Li et al., 2020; Vidal-Macua et al., 2020; Yang et al., 2018). A national project, China Mining Geological Environment Remote Sensing Monitoring, started in 2010, can monitor the spatial distribution of almost all mine restoration areas in China, but the project adopts the visual interpretation method, which is time-consuming. As only the current year is assessed each year, it is also difficult to track recovery over multiple years and make the monitoring data available to common researchers.

GEE platform is an effective tool for completing the processing of thousands of Landsat images used for mine sites' restoration monitoring. The GEE platform synchronizes all USGS Landsat series data. Different levels of processing products can be used, including raw data, TOA, SR data, and composite products. Based on the GEE platform researchers have achieved a great deal in forest monitoring, urban sprawl monitoring, and ecosystem monitoring on a regional and even global scale (Dong et al., 2016; Gumma et al., 2019; Hansen et al., 2013; Kennedy, Yang, & Cohen, 2010; Xiaoping Liu et al., 2018; Phalke et al., 2020). Benefiting from researchers' contributions and improvements in the computing codes, more and more functions are implemented on the GEE platform, greatly improving the

accuracy and speed of data processing (Ermida, Soares, Mantas, Göttsche, & Trigo, 2020). Until the completion of this study, the open source code based on the Landsat series of images for computing LST was presented (Ermida et al., 2020). This code can be used if future studies using MLRI place a higher demand on LST.

The MLRI constructed in this study is promising on restoration monitoring. The MLRI index calculated at the pixel scale is compared to the historical state of that pixel, avoiding differences due to vegetation type, elevation, climatic conditions, etc. Therefore, the use of this index to monitor the mine site restoration process can be used simultaneously in different mine sites. This is an important reason why this study selected so many mine sites in the northwestern ecologically fragile region of China for restoration monitoring.

4.2 The effectiveness of Green Mines construction and land reclamation

In 2011, the State Council of China promulgated “the Land Reclamation Regulations”, making it clear that all land damaged or destroyed by production and construction activities must be reclaimed. In accordance with the principle of "whoever destroys the land, whoever reclaims it", the producer or builder is responsible for its reclamation. For damaged and destroyed land left over from history where the producer cannot be identified, the government is responsible for reclaiming the land. In the same year, the Ministry of Land and Resources announced the first batch of pilot green mines. 2017, the Ministry of Land and Resources and six other ministries jointly issued the "Implementation Opinions on Accelerating the Construction of Green Mines" clearly pointed out that a new pattern of Green Mines construction should be basically formed, and strive to form a new model of mining development in line with the requirements of Ecological Civilization construction by 2020. There have been studies showing that some of the mine sites are well restored, with vegetation in some areas reaching or even exceeding pre-mining levels (Huang et al., 2016; J.

Li et al., 2020). The results of this paper should confirm the effectiveness of China's ambitious green mine construction. However, according to the restored area predictions in this paper, there are still some areas in the restored area that are at risk of degradation. Mine builders should screen for effective restoration measures and strengthen the maintenance of restoration results.

One of our conclusions is that the effects of mine restoration are positively correlated with the duration of mining. A possible explanation is that mine restoration requires significant financial investment (Bruno Rocha Martins et al., 2020; Lechner et al., 2017). Usually mines with longer mining duration have more stable financial status and more experience in management to support mine restoration projects. Therefore, the development of a new mine plan requires not only the need to measure the cumulative, social, and environmental impacts of mining in an integrated manner, but also the long-term economic value of the mined resource.

4.3 Uncertainty analysis and implications for extensive applications

In selecting the mine sites for this study, the extents of some mine sites in the Zhundong coal base were mapped. However, considering that the surface cover of the area is mainly chestnut calcareous and the vegetation cover is very poor, these mine sites were not included in the study. The suitability of the MLRI with EVI as a very important component for use in the area is not yet known. Subsequent research can focus on the area of application of MLRI. In this study, the GEE platform was used to calculate the LST and EVI. but the MLRI construction and restoration types classification were still done on the local computer's ArcGIS platform. If more of the research process could be done on the GEE platform in the future, it would significantly reduce research time. In addition, this study validated the accuracy of the identification of restoration areas, but only classified the two restoration types

based on the results of the Hurst index calculations, and no study has yet achieved the validation of future trends. If the ecosystem in the restored area of the mine had become very stable before 2000, our study might not have identified these restoration processes. To our knowledge, such areas are very few in our study area.

DRDI is an important basis for presenting MLRI, which can accurately identify disturbances in the restoration process. DRDI needs to be used under the condition that the restoration area is clearly defined, otherwise it is difficult to determine whether the disturbance is occurring in the restoration area. The MLRI is proposed to fill the gap. In subsequent studies, the MLRI and DRDI can be used together to monitor the disturbance and restoration of the mine site. After using a reference ecosystem to determine the threshold value of the MLRI for changes in natural state and anthropogenic restoration, the MLRI also has the potential to identify the restoration that occurs in each year. Hence, using the index to identify the time of mine restoration occurs more accurately is also desirable.

5.Conclusion

In order to achieve monitoring of multiple surface coal mine restoration in a large scale, this study constructed a new index MLRI for monitoring mine site restoration, which couples Land Surface Temperature (LST) and Enhanced Vegetation Index (EVI). The LST and EVI data calculations required for the study were completed on the GEE platform, based on 3675 Landsat images. Time series analysis of the MLRI enabled identification and localization of restoration areas. A dataset of restoration areas and restoration processes was created for 46 mine sites located in the northwestern ecologically fragile region of China from 2000 to 2019. In terms of overall restoration effects, the percentage of restoration area was significantly higher in mines that started mining before 2000 than after 2000. And the restoration effect of mine area is positively correlated with the duration of mining. According to the restoration

effects, the 46 sites were clustered into high, medium, and low restoration area percentage clusters with 13, 11, and 22 mine sites, respectively. Mine sites with the high percentage of restoration area are mainly located in Shengli&Huolinhe and Shanbeimengnan region of the six mine regions. region (Shengli&Huolinhe) The mine sites with medium and low percentages of restoration area can be found in Hailar, Shengli&Huolinhe, Yuanbaoshan, Shanbeimengnan, and Zhuozishan&Luotuoshan region, and all mines in Zhunnan region have low percentages of restoration area. The results of this paper should confirm the effectiveness of China's ambitious green mine construction. And mine builders should screen for effective restoration measures to enhance the maintenance of the restoration results and prevent further degradation of the restored area. Monitoring restoration of surface coal mine sites with MLRI will support regional mine restoration programs and sustainable mining development planning.

References

Bian, Z., & Lu, Q. (2012). Ecological effects analysis of land use change in coal mining area based on ecosystem service valuing: a case study in Jiawang. *Environmental Earth Sciences, 68*(6), 1619-1630. doi:10.1007/s12665-012-1855-0

Bruno Rocha Martins, W., Douglas Roque Lima, M., de Oliveira Barros Junior, U., Sousa Villas-Boas Amorim, L., de Assis Oliveira, F., & Schwartz, G. (2020). Ecological methods and indicators for recovering and monitoring ecosystems after mining: A global literature review. *Ecological Engineering, 145*, 105707. doi:10.1016/j.ecoleng.2019.105707

Cross, A. T., Young, R., Nevill, P., McDonald, T., Prach, K., Aronson, J., . . . Dixon, K. W. (2018). Appropriate aspirations for effective post-mining restoration and rehabilitation: a response to Kaźmierczak et al. *Environmental Earth Sciences, 77*(6), 256. doi:10.1007/s12665-018-7437-z

Dong, J., Xiao, X., Menarguez, M. A., Zhang, G., Qin, Y., Thau, D., . . . Moore, B., 3rd. (2016). Mapping paddy rice planting area in northeastern Asia with Landsat 8 images, phenology-based algorithm and Google Earth Engine. *Remote Sensing of Environment, 185*, 142-154. doi:10.1016/j.rse.2016.02.016

Ermida, S. L., Soares, P., Mantas, V., Göttsche, F.-M., & Trigo, I. F. (2020). Google Earth Engine Open-Source Code for Land Surface Temperature Estimation from the Landsat Series. *Remote Sensing, 12*, 1471. doi:10.3390/rs12091471

Feng, Y., Wang, J., Bai, Z., & Reading, L. (2019). Effects of surface coal mining and land reclamation on soil properties: A review. *Earth-Science Reviews, 191*, 12-25. doi:10.1016/j.earscirev.2019.02.015

Freitas, M. G., Rodrigues, S. B., Campos-Filho, E. M., do Carmo, G. H. P., da Veiga, J. M., Junqueira, R. G. P., & Vieira, D. L. M. (2019). Evaluating the success of direct seeding for tropical forest restoration over ten years. *Forest Ecology and Management, 438*, 224-232. doi:10.1016/j.foreco.2019.02.024

Gumma, M. K., Thenkabail, P. S., Teluguntla, P. G., Oliphant, A., Xiong, J., Giri, C., . . . Whitbread, A. M. (2019). Agricultural cropland extent and areas of South Asia derived using Landsat satellite 30-m time-series big-data using random forest machine learning algorithms on the Google Earth Engine cloud. *GIScience & Remote Sensing, 57*(3), 302-322. doi:10.1080/15481603.2019.1690780

Hansen, M. C., Potapov, P. V., Moore, R., Hancher, M., Turubanova, S. A., Tyukavina, A., . . . Townshend, J. R. G. (2013). High-resolution global maps of 21st-century forest cover change. *Science, 342*(15), 850-885.

Hilson, G. (2002). An overview of land use conflicts in mining communities. *Land Use Policy, 19*, 65-73.

Hobbs, R., & Harris, J. (2001). Restoration Ecology: Repairing the Earth's Ecosystems in the New Millennium. *Restoration Ecology, 9*(2), 239-246.

Hu, Z. (2019). The 30 years'land reclamation and ecological restoration in China: review , rethinking and prospect. *Coal Science and Technology (In Chinese), 47*(1), 25-35. doi:doi: 10. 13199 / j. cnki. cst. 2019. 01. 004

Huang, L., Zhang, P., Hu, Y., & Zhao, Y. (2016). Vegetation and soil restoration in refuse dumps from open pit coal mines. *Ecological Engineering, 94*, 638-646. doi:10.1016/j.ecoleng.2016.06.108

Intergovernmental Science-Policy Platform on Biodiversity and Ecosystem Services. (2018). *The IPBES assessment report on land degradation and restoration.* Bonn, Germany: Secretariat of the Intergovernmental Science-Policy Platform on Biodiversity and Ecosystem Services.

International Energy Agency. (2020). Coal Information: Overview. Retrieved from https://www.iea.org/reports/coal-information-overview

International Geosphere-Biosphere Programme. (2005). *GLP:Science Plan and Implementation Strategy.* Stockholm: IGBP Secretariat.

Karan, S. K., Samadder, S. R., & Maiti, S. K. (2016). Assessment of the capability of remote sensing and GIS techniques for monitoring reclamation success in coal mine degraded lands. *Journal of Environmental Management, 182*, 272-283. doi:10.1016/j.jenvman.2016.07.070

Kendall, M. G. (1970). *Rank Correlation Methods*. London: Oxford University Press.

Kennedy, R. E., Yang, Z., & Cohen, W. B. (2010). Detecting trends in forest disturbance and recovery using yearly Landsat time series: 1. LandTrendr — Temporal segmentation algorithms. *Remote Sensing of Environment, 114*(12), 2897-2910. doi:10.1016/j.rse.2010.07.008

Lechner, A. M., McIntyre, N., Witt, K., Raymond, C. M., Arnold, S., Scott, M., & Rifkin, W. (2017). Challenges of integrated modelling in mining regions to address social, environmental and economic impacts. *Environmental Modelling & Software, 93*, 268-281. doi:10.1016/j.envsoft.2017.03.020

Li, H., She, C., Zhou, Y., & Huang, Y. (2019). Summary and prospect of open-pit coal mining technology in China. *Coal Science and Technology (In Chinese), 47*(10), 24-35. doi:doi: 10. 13199 /j. cnki. cst. 2019. 10. 002

Li, J., Yan, X., Cao, Z., Yang, Z., Liang, J., Ma, T., & Liu, Q. (2020). Identification of successional trajectory over 30 Years and evaluation of reclamation effect in coal waste dumps of surface coal mine. *Journal of Cleaner Production, 269*, 122161.

doi:10.1016/j.jclepro.2020.122161
Liu, S., Li, W., Qiao, W., Wang, Q., Hu, Y., & Wang, Z. (2019). Effect of natural conditions and mining activities on vegetation variations in arid and semiarid mining regions. *Ecological Indicators, 103*, 331-345. doi:10.1016/j.ecolind.2019.04.034
Liu, X., Hu, G., Chen, Y., Li, X., Xu, X., Li, S., . . . Wang, S. (2018). High-resolution multi-temporal mapping of global urban land using Landsat images based on the Google Earth Engine Platform. *Remote Sensing of Environment, 209*, 227-239. doi:10.1016/j.rse.2018.02.055
Liu, X., Zhou, W., & Bai, Z. (2016). Vegetation coverage change and stability in large open-pit coal mine dumps in China during 1990–2015. *Ecological Engineering, 95*, 447-451. doi:10.1016/j.ecoleng.2016.06.051
Macdonald, S. E., Landhäusser, S. M., Skousen, J., Franklin, J., Frouz, J., Hall, S., . . . Quideau, S. (2015). Forest restoration following surface mining disturbance: challenges and solutions. *New Forests, 46*(5-6), 703-732. doi:10.1007/s11056-015-9506-4
Mann, H. B. (1945). Nonparametric test against trend. *Econometrica, 13*, 245–259.
Mildrexler, D. J., Zhao, M., Heinsch, F. A., & Running, S. W. (2007). A new satellite-based methodology for continental-scale disturbance detection. *Ecological Applications, 17*(1), 235–250.
Mildrexler, D. J., Zhao, M., & Running, S. W. (2009). Testing a MODIS Global Disturbance Index across North America. *Remote Sensing of Environment, 113*(10), 2103-2117. doi:10.1016/j.rse.2009.05.016
Millennium Ecosystem Assessment. (2005). *Ecosystems and Human Well-Being: Synthesis*. Washington: Island Press.
Moomen, A.-W., Bertolotto, M., Lacroix, P., & Jensen, D. (2019). Inadequate adaptation of geospatial information for sustainable mining towards agenda 2030 sustainable development goals. *Journal of Cleaner Production, 238*, 117954. doi:10.1016/j.jclepro.2019.117954
National Energy Administration. (2016). Thirteen Five-Year Plan for Coal Industry Development. Retrieved from http://www.nea.gov.cn/2016-12/30/c_135944439.htm
National Energy Administration. (2019). Announcement No. 2 of 2019. Retrieved from http://zfxxgk.nea.gov.cn/auto85/201903/t20190326_3637.htm
Nemani, R., & Running, S. (1997). Land Cover Characterization Using Multitemporal Red, Near-IR, and Thermal-IR Data from NOAA/AVHRR. *Ecological Applications, 7*(1), 79-90.
Peng, J., Liu, Z., Liu, Y., Wu, J., & Han, Y. (2012). Trend analysis of vegetation dynamics in Qinghai–Tibet Plateau using Hurst Exponent. *Ecological Indicators, 14*(1), 28-39. doi:10.1016/j.ecolind.2011.08.011
Phalke, A. R., Özdoğan, M., Thenkabail, P. S., Erickson, T., Gorelick, N., Yadav, K., & Congalton, R. G. (2020). Mapping croplands of Europe, Middle East, Russia, and Central Asia using Landsat, Random Forest, and Google Earth Engine. *ISPRS Journal of Photogrammetry and Remote Sensing, 167*, 104-122. doi:10.1016/j.isprsjprs.2020.06.022
Sen, S., Zipper, C. E., Wynne, R. H., & Donovan, P. F. (2012). Identifying Revegetated Mines as Disturbance/Recovery Trajectories Using an Interannual Landsat Chronosequence. *Photogrammetric Engineering & Remote Sensing, 70*(3), 223–235.
Sobrino, J. A., Jiménez-Muñoz, J. C., & Paolini, L. (2004). Land surface temperature retrieval from LANDSAT TM 5. *Remote Sensing of Environment, 90*(4), 434-440. doi:10.1016/j.rse.2004.02.003

Song, W., Song, W., Gu, H., & Li, F. (2020). Progress in the Remote Sensing Monitoring of the Ecological Environment in Mining Areas. *Int J Environ Res Public Health, 17*, 1846. doi:10.3390/ijerph17061846

United Nations. (2015). Transfoming our wolrd: The 2030 agenda for sustainable development. Retrieved from https://sustainabledevelopment.un.org/post2015/transformingourworld/publication

United States Geological Survey. (2016). Landsat 8 Data Users Handbook. Retrieved from https://www.usgs.gov/core-science-systems/nli/landsat/landsat-8-data-users-handbook

Vidal-Macua, J. J., Nicolau, J. M., Vicente, E., & Moreno-de Las Heras, M. (2020). Assessing vegetation recovery in reclaimed opencast mines of the Teruel coalfield (Spain) using Landsat time series and boosted regression trees. *Science of the Total Environment, 717*, 137250. doi:10.1016/j.scitotenv.2020.137250

Wang, L., Diao, C., Xian, G., Yin, D., Lu, Y., Zou, S., & Erickson, T. A. (2020). A summary of the special issue on remote sensing of land change science with Google earth engine. *Remote Sensing of Environment, 248*, 112002. doi:10.1016/j.rse.2020.112002

Werner, T. T., Mudd, G. M., Schipper, A. M., Huijbregts, M. A. J., Taneja, L., & Northey, S. A. (2020). Global-scale remote sensing of mine areas and analysis of factors explaining their extent. *Global Environmental Change, 60*, 102007. doi:10.1016/j.gloenvcha.2019.102007

Wu, X., Lv, X., Zhao, Y., Sun, H., & Li, J. (2020). Ecological resilience assessment of an arid coal mining area using index of entropy and linear weighted analysis: A case study of Shendong Coalfield, China. *Ecological Indicators, 109*, 105843. doi:10.1016/j.ecolind.2019.105843

Xie, M., Gao, S., Li, S., Zhou, Y., Bai, Z., & Zhang, Y. (2019). Construction and spatiotemporal variation of dump reclamation disturbance index. *Transactions of the Chinese Society of Agricultural Engineering (In Chinese), 35*(23), 258-265. doi:10.11975/j.issn.1002-6819.2019.23.032

Yang, Y., Erskine, P. D., Lechner, A. M., Mulligan, D., Zhang, S., & Wang, Z. (2018). Detecting the dynamics of vegetation disturbance and recovery in surface mining area via Landsat imagery and LandTrendr algorithm. *Journal of Cleaner Production, 178*, 353-362. doi:10.1016/j.jclepro.2018.01.050

Yu, L., Xu, Y., Xue, Y., Li, X., Cheng, Y., Liu, X., . . . Gong, P. (2018). Monitoring surface mining belts using multiple remote sensing datasets: A global perspective. *Ore Geology Reviews, 101*, 675-687. doi:10.1016/j.oregeorev.2018.08.019

Zhang, L., Wang, J., Bai, Z., & Lv, C. (2015). Effects of vegetation on runoff and soil erosion on reclaimed land in an opencast coal-mine dump in a loess area. *Catena, 128*, 44-53. doi:10.1016/j.catena.2015.01.016

Zhou, B., Okin, G. S., & Zhang, J. (2020). Leveraging Google Earth Engine (GEE) and machine learning algorithms to incorporate in situ measurement from different times for rangelands monitoring. *Remote Sensing of Environment, 236*, 111521. doi:10.1016/j.rse.2019.111521

Zhou, Z., Ding, Y., Shi, H., Cai, H., Fu, Q., Liu, S., & Li, T. (2020). Analysis and prediction of vegetation dynamic changes in China: Past, present and future. *Ecological Indicators, 117*, 106642. doi:10.1016/j.ecolind.2020.106642

94

703 Tables

704 **TABLE 1** Mine sites information of this study.

Mine regions	No.	Mine Site name	Area/hm^2	Mining start time
Hailar region	1	Yimin	2887.64	Before 2000
(Mine region1,7 mine sites)	2	Lingquan	2876.34	Before 2000
	3	BaorixileI	2297.88	Before 2000
	4	BaorixileII	733.99	2004
	5	Zhanihe	702.63	2010
	6	Mianduhexi	409.29	Before 2000
	7	Xieertala&Shunxing	299.95	Before 2000
Shengli&Huolinhe region	8	Huolinhenan	5053.58	Before 2000
(Mine region2,15 mine sites)	9	Zhahanaoer	4116.16	Before 2000
	10	BaiyinhuaI&II	3654.87	2008
	11	ShenglidongII	3549.61	2008
	12	Hesigelawu	3104.06	2008
	13	Baorihushuo	2368.73	2006
	14	ShenglixiI	2183.69	Before 2000
	15	BaiyinhuaIII	1928.56	2009
	16	BaiyinhuaIV	1585.40	2009
	17	Fengyang	1550.27	Before 2000
	18	Shenglixier	1452.53	2007
	19	Huolinhebei	1121.31	Before 2000
	20	JilinguoleII	802.80	2011
	21	ShenglixiIII	533.96	2008
	22	Hadatu	311.84	Before 2000
Yuanbaoshan region	23	Pingzhuangxi	1758.22	Before 2000
(Mine region3, 2mine sites)	24	Yuanbaoshan	1613.96	Before 2000
Shanbeimengnan region	25	Anjialing&Antaibao	8268.35	Before 2000
(Mine region4, 12 mine sites)	26	Heidaigou&Haerwusu	5729.04	Before 2000
	27	Daqingshan	4481.39	2010
	28	Pingshuodong	2044.90	2008
	29	Wujiata	1822.38	Before 2000
	30	Weijiamao	992.34	2012
	31	Xiwan	925.06	2016
	32	Dongshanwan	491.39	2010
	33	Datangbaoli	355.15	2007
	34	Majiata	265.42	Before 2000
	35	Bijian	228.12	2010
	36	Shuiquan	201.63	2008
Zhuozishan&Luotuoshan region	37	Luotuoshan	25941.68	Before 2000

(Mine region5, 7 mine sites)	38	Dafeng	10305.08	Before 2000
	39	Haibowan	5569.27	Before 2000
	40	Maliantan	3111.36	Before 2000
	41	Caiyuangou	1074.46	Before 2000
	42	HaibowanII	420.82	2007
	43	Qingshuigou	263.99	Before 2000
Zhunnan region	44	Heishan	1144.35	Before 2000
(Mine region6, 3 mine sites)	45	Heishanxiao	913.99	2009
	46	Tuokexun	371.85	2009

TABLE 2 Principles of Restoration types classification.

Restoration types	Mann-Kendall test	Slope	H-value
Significant Consistent Increase (SCI)	>|1.96|	>0	>0.5
Significant Anti-consistent Increase (SAI)			≤0.5

TABLE 3 The accuracy of the detected restoration

Mine site	Significant increase		Other trends		Overall accuracy	Kappa coefficient
	Producer's accuracy	User's accuracy	Producer's accuracy	User's accuracy		
Antaibao&Anjialing	0.98	0.93	0.87	0.97	0.94	0.88
ShenglixiIII	0.81	0.86	0.98	0.96	0.95	0.81

TABLE 4 Percentages of the area of restoration types at Antaibao&Anjialing and ShenglixiIII mine sites

Restoration types	Antaibao&Anjialing	ShenglixiIII
	Percentage of area/%	Percentage of area/%
Significant consistent increase (SCI)	42.68	14.94
Significant anti-consistent increase (SAI)	21.47	4.39
Significant increase (SI)	64.25	19.33

Figures

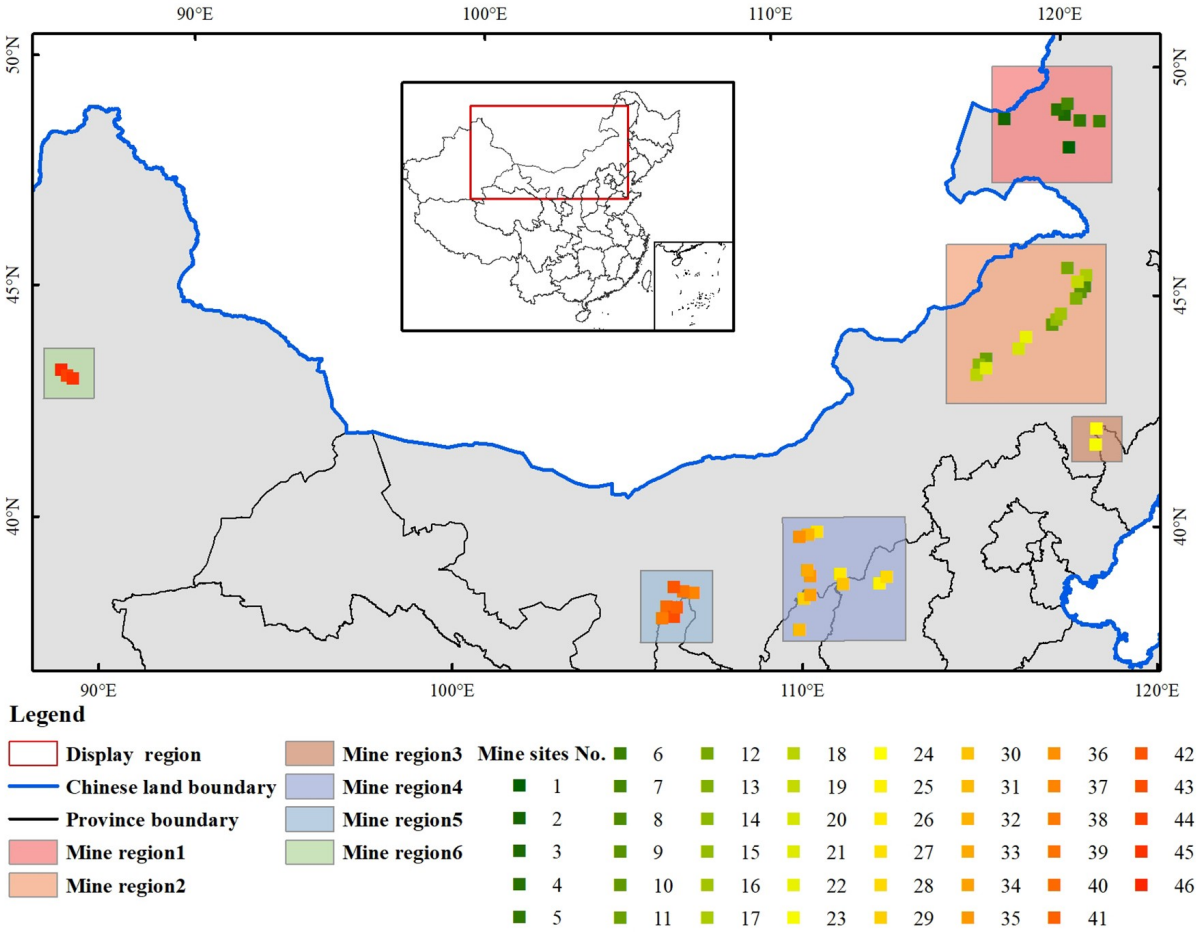

FIGURE 1 Mines mapped and analyzed in this study. The names of the six mine regions are: mine region1 = Hailar region, mine region 2 = Shengli&Huolinhe region, mine region3 = Yuanbaoshan region, mine region4 = Shanbeimengnan region, mine region5 = Zhuozishan&Luotuoshan region, mine region6 = Zhunnan region.

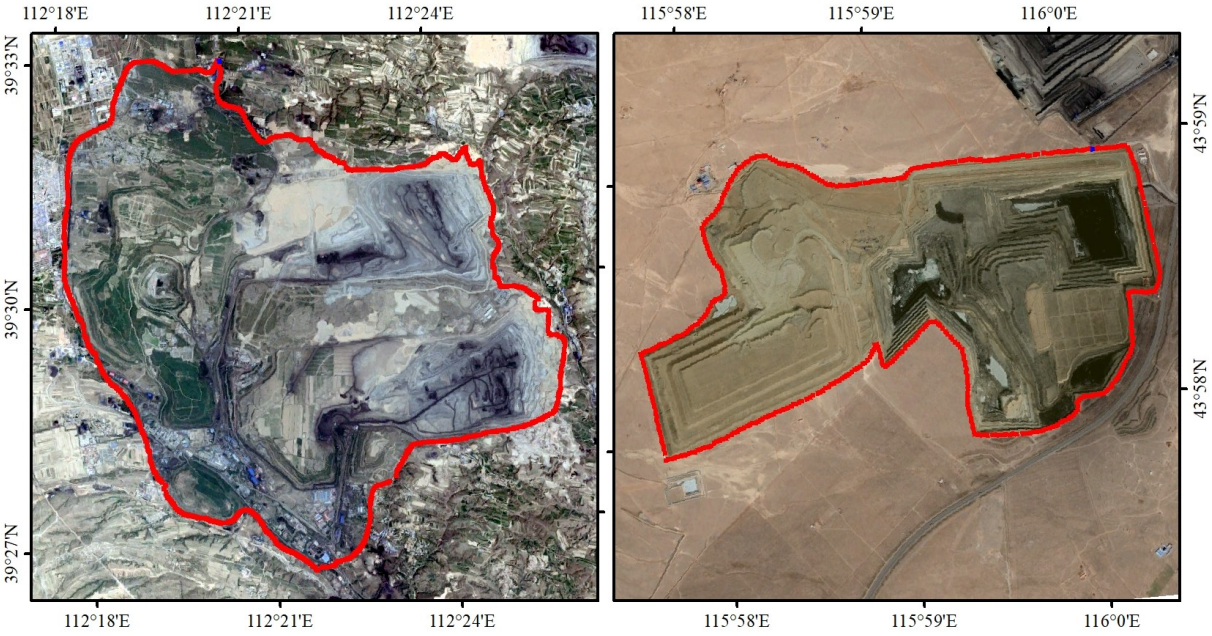

FIGURE 2 Surface mine site extents of Antaibao&Anjialing (left) and ShenglixiIII (right).

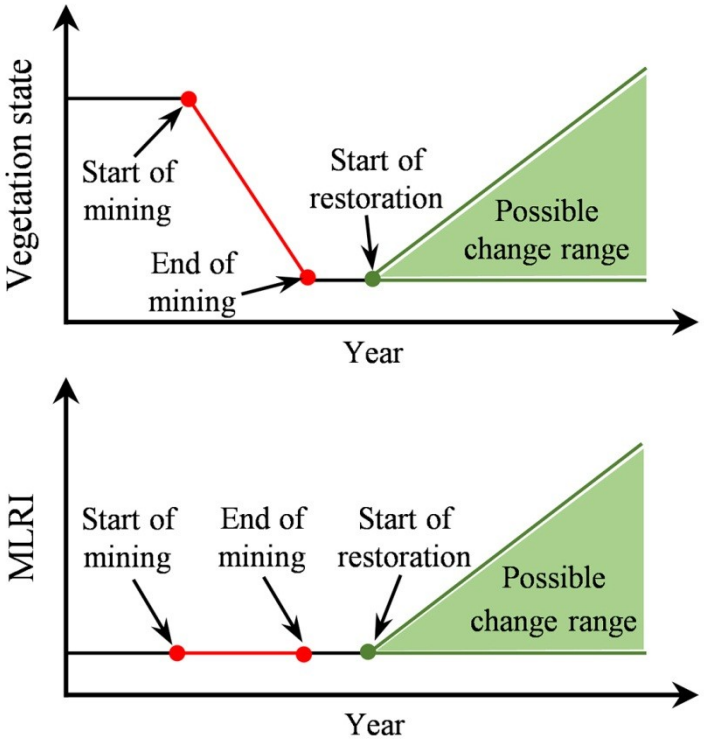

FIGURE 3 A conceptual model for the trajectory of vegetation state and MLRI for a pixel.

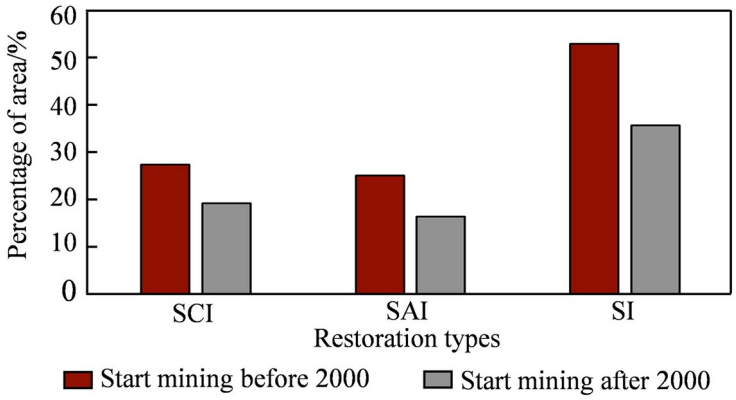

FIGURE 4 Area percentage of restoration types area different start mining time

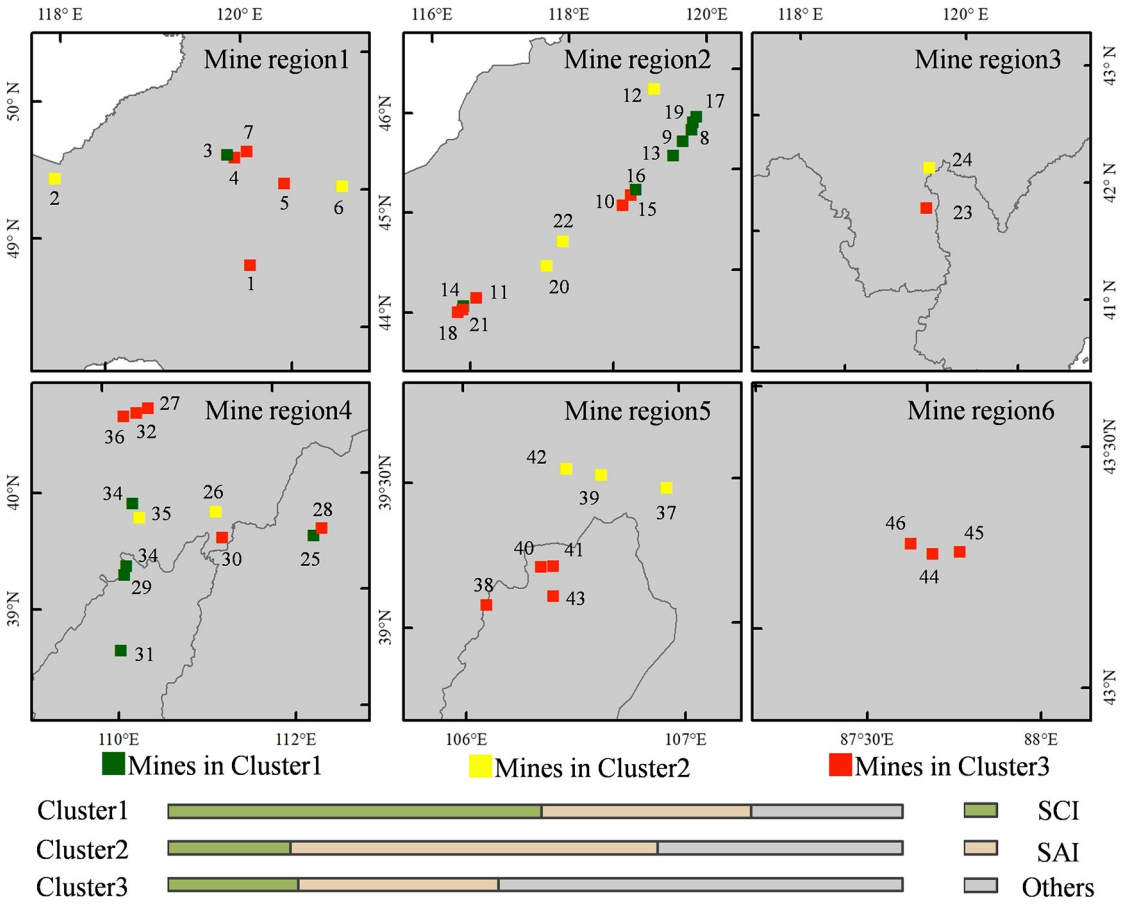

FIGURE 5 The distribution of mines in three clusters.

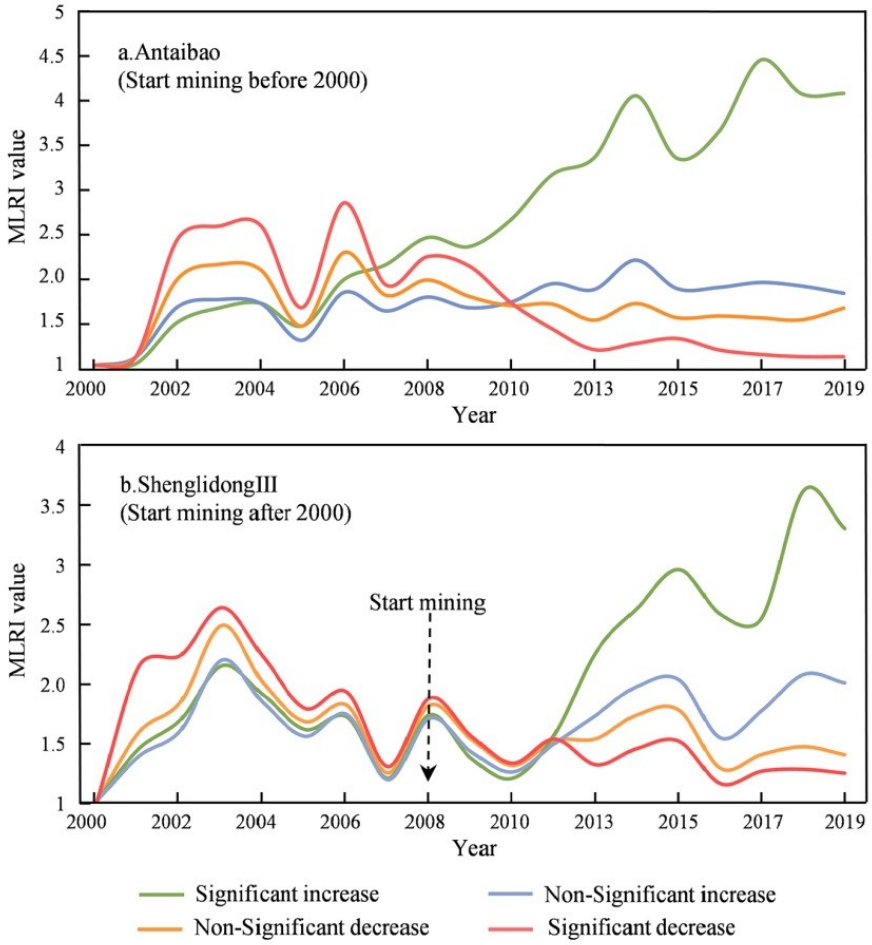

FIGURE 6 MLRI changes of Antaibao&Anjialing and ShenglixiIII.

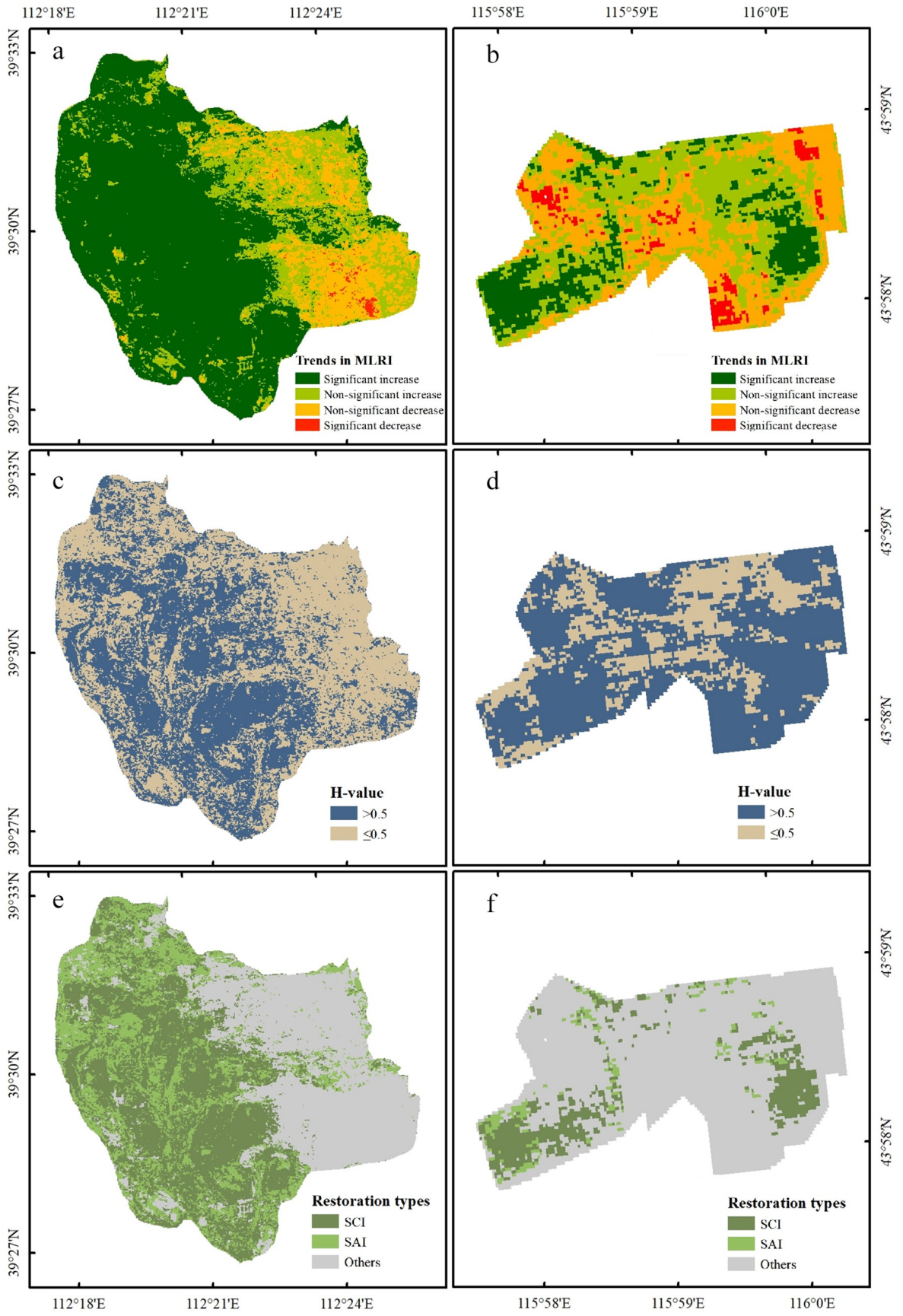

FIGURE 7 Details of the spatial distribution of restoration types of Antaibao&Anjialing (left) and

115

737 ShenglixiIII (right) from 2000 to 2019.

738 Supplemental Material

739

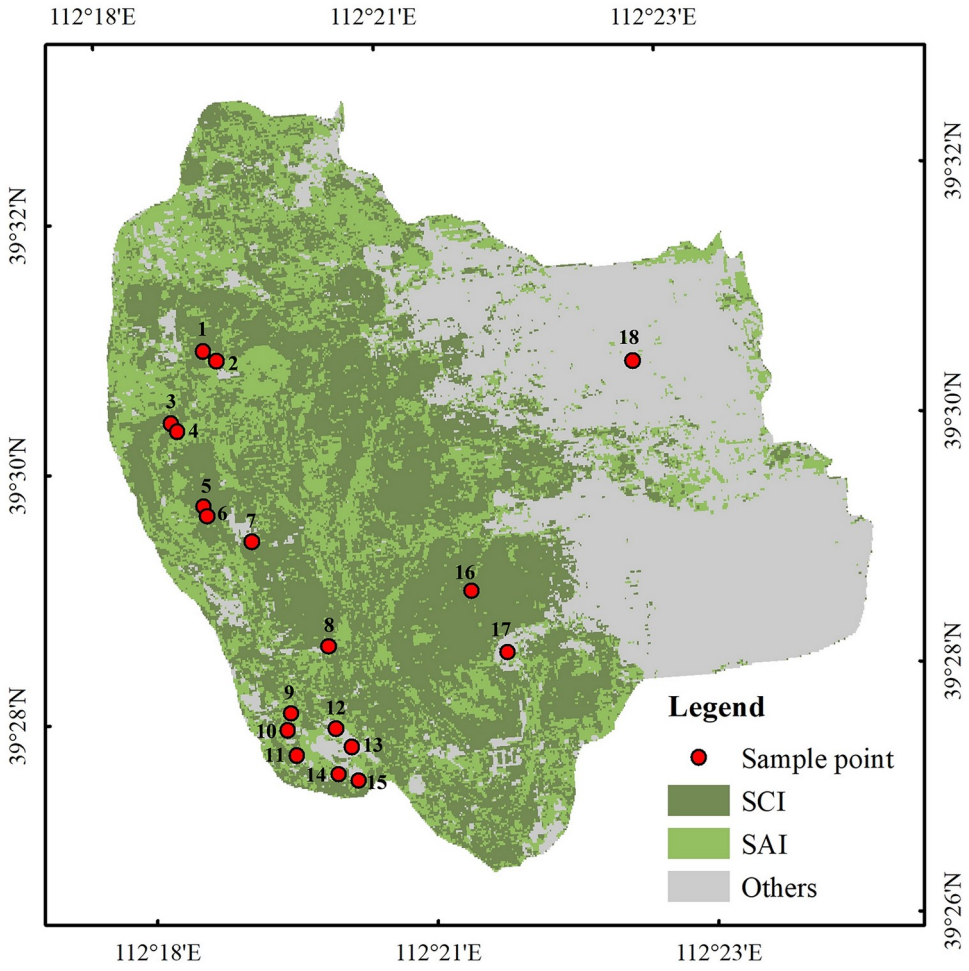

740

741 FIGURE S1. Distribution of field validated sampling sites.

742

FIGURE S2. Sample point 1. Identified as restoration area, verified as grassland. Shot on 10/10/2020.

FIGURE S3. Sample point 2. Identified as restoration area, verified as grassland. Shot on 10/10/2020.

FIGURE S4. Sample point 3. Identified as restoration area, verified as shrubland. Shot on 10/10/2020.

FIGURE S5. Sample point 4. Identified as restoration area, verified as grassland. Shot on 10/10/2020.

FIGURE S6. Sample point 5. Identified as restoration area, verified as forest land. Shot on 10/10/2020.

FIGURE S7. Sample point 6. Identified as restoration area, verified as shrubland. Shot on 10/10/2020.

FIGURE S8. Sample point 7. Identified as restoration area, verified as forest land. Shot on 10/10/2020.

FIGURE S9. Sample point 8. Identified as restoration area, verified as forest land. Shot on 10/10/2020.

FIGURE S10. Sample point 9. Identified as restoration area, verified as grassland. Shot on 10/10/2020.

FIGURE S11. Sample point 10. Identified as restoration area, verified as grassland. Shot on 10/10/2020. There is spontaneous combustion of coal waste in the area, making it difficult for trees to survive.

FIGURE S12. Sample point 11. Identified as restoration area, verified as forest land. Shot on 10/10/2020.

FIGURE S13. Sample point 12. Identified as restoration area, verified as forest land. Shot on 10/10/2020.

FIGURE S14. Sample point 13. Identified as unrestored area, verified as forest land. Shot on 10/10/2020. Communication with mine plant staff revealed that restoration of the ecosystem in the area began in 1990 and that the ecosystem reached a stable state before 2000.

FIGURE S15. Sample point 14. Identified as restoration area, verified as shrubland. Shot on 10/10/2020.

FIGURE S16. Sample point 15. Identified as restoration area, verified as forest land. Shot on 10/10/2020.

FIGURE S17. Sample point 16. Identified as restoration area, verified as grassland. Shot on 10/10/2020.

FIGURE S18. Sample point 17. Identified as unrestored area, verified as mining land. Shot on 10/10/2020.

FIGURE S19. Sample point 18. Identified as unrestored area, verified as mining land. Shot on 10/10/2020.